Quantifying Information Transfer in Chiral Floquet Phases

an honors thesis
by
Blake Duschatko
to
The Physics Department

in partial fulfillment of the requirements
for the degree of
Bachelor of Science with Honors
in the subject of
Physics

The University of Texas
Austin, Texas
May 2018

Thesis advisor: Andrew Potter Blake Duschatko

Quantifying Information Transfer in Chiral Floquet Phases

Abstract

Complex quantum systems have become an increasingly fascinating area of research. Their exotic behavior, which differs so drastically from classical systems, gives rise to a large range of novel phases of matter. In particular, it has been recently understood that the many body localization phenomenon, along with Floquet driving, can endow quantum systems with out of equilibrium dynamics that are unattainable in static settings. These and other topological condensed matter systems have begun to drive research in quantum matter.

The subsequent study examines a class of two dimensional phases of matter known as chiral Floquet phases. These quantum systems exhibit chiral edge modes that serve as a one way transport of quantum information. Strikingly, this information flow is precisely quantized and protected against local perturbations. Unlike examples such as the quantum Hall effect, the existence of quantized information transfer results from dynamical motion of quantum states rather than some conserved quantity. Expanding the existing body of knowledge on these phases allows for the possibility of realizing their implementation in quantum information processing.

The ensuing work begins with a historical and technical overview of the principles of topological phases of matter, followed by an examination of Floquet systems. This will lead directly into a discussion of chiral Floquet phases and their characterizations, along with a novel study of new means for quantifying their edge states. This new research avenue raises the possibility of experimentally characterizing chiral Floquet phases, which until now have been restricted to theoretical studies. Moreover, it will provide a more physically transparent way of understanding the dynamics of these systems.

Contents

Conventions and Previous Work

This work is largely based on the contents of

B. R. Duschatko, P. T. Dumitrescu, and A. C. Potter, ArXiv e-prints (2018), arXiv:1804.02004 [cond-mat.str-el].

In particular, the contents of section 2 represents a more detailed analysis than that presented in the above work.

Throughout the text we will adopt the convention that $\hbar = k_b = 1$, and that the Pauli spin operators are expressed as $\vec{S} = \frac{1}{2}\vec{\sigma}$. Unless the context of the problem makes it unclear, the hat over operators will be omitted such that $\hat{\mathcal{O}} \equiv \mathcal{O}$.

Acknowledgments

I am, first and foremost, ever so thankful for the guidance from my research supervisor, Dr. Andrew Potter. Our interactions have been entirely transformative in the way that I now approach problems in physics. Moreover, my research interests and approach have been positively influenced by our discussions throughout the past year.

I would also like to extend thanks to Dr. Philipp Dumitrescu, whose conversations and input have led to new new research avenues. His physical intuition for many complex problems has been an essential tool in progressing my understanding of condensed matter problems.

A special thanks is due to Dr. Can Kilic and Dr. Greg Sitz for their continued support throughout my undergraduate career. They have, along with Dr. Potter, been encouraging in my establishment of a research identity. It is with their continuous feedback that I have been able to find a voice in physics and research avenues that resonant with me intellectually.

Additionally, I wish to express my utmost gratitude to my many peers; Alex, Avery, Lucas, Jonathan, and many others. Though our career goals differ greatly, our many conversations have aided me in making numerous difficult decisions throughout my studies.

Finally, my deepest thanks to my family and my fiancée, Autumn. Their love, support, encouragement, and emotional grounding have been essential in my success over the course of my undergraduate studies.

1 Introduction

Condensed matter research has traditionally been geared towards studies of system ground states and their low-lying excitations in thermal equilibrium. Through these studies, a wide range of topological phases of matter have been discovered. In contrast to symmetry-breaking phases of matter such as magnets, topological phases cannot be described by any local order parameter. Further, they possess surface states with strikingly robust properties, and these phases have important implications for advances in quantum technologies, such as fault tolerant quantum computing [1].

One of the most well known examples of an equilibrium topological phase is the integer quantum hall effect (IQHE). The physics of IQH states has been studied exhaustively; they have been shown to exhibit chiral edge modes when a system edge is exposed that transport electric charge, and different IQH phases are characterized by a quantized Hall conductance. The IQHE is well understood and represents a stepping stone into the physical world of more complex topological phases.

Despite their interesting properties, IQH systems themselves are only found in equilibrium

settings in the limit of zero temperature. In light of the recent progress in experimental atomic, molecular, and optical (AMO) settings, as well as superconducting qubit systems, the exploration of dynamical topological phases in systems driven far from equilibrium have dominated recent theoretical efforts [2–13]. This new realm of excited state physics reveals a host of phases with intriguing properties beyond those of IQH systems..

This work will explore chiral Floquet (CF) phases, a particularly impactful set of out of equilibrium topological phases [2–7]. In sharp contrast to IQH systems, CF phases are inherently dynamical and are not realized in equilibrium settings. These two sets of topological phases do possess some similarities, as the CF phases exhibit chiral edge modes. A key difference, however, is that the edge modes of a CF phase do not carry locally observable quantities such as heat or charge, as in IQH systems. Rather, the quantum states of the system are transported along the edge in quantized amounts, described by a topological invariant known as the chiral unitary index.

Distinguishing different edge states with the chiral unitary index is presently a challenge in some ways. While the current characterization in terms of operator algebra overlaps [5, 14] and matrix product operators [5, 15, 16] serve as useful theoretical tools, they are arguably unintuitive. More importantly, such topological invariants cannot be realistically be measured in an experimental setting. In this work, we develop a new quantity, the chiral mutual information, which describes the edge modes of a CF phase in terms of entanglement entropies. These can be experimentally measured using interferometric techniques [17, 18], and we will consider an experimental protocol for the chiral mutual information scheme.

This section in particular will develop the principal concepts of equilibrium topological phases for the purpose of understanding their non-equilibrium counterparts. Beginning with a brief exploration of the IQHE, we will transition into an overview of equilibrium physics in closed quantum systems. Building on this, we will examine how the physics of topological phases changes in systems driven far from equilibrium. These tools will allow for the introduction of chiral Floquet models which serve as the backbone for the novel work in this thesis.

1.1 Integer Quantum Hall Effect

The first example of topological phases we will explore are integer quantum Hall systems. Unlike traditional phases of matter which can be described by symmetry breaking and local order

parameters, there is something inherently global about the structure of IQH states. In fact, this is a defining feature of all topological phases and requires that they be described by a topologically invariant quantity. Generally speaking, a topological phase transition can occur when tuning system parameters, where energy gaps close, even without a symmetry being broken. While strictly an equilibrium phenomenon, well defined in the zero temperature limit, investigating the properties of IQH systems will set a context for understanding out of equilibrium phases.

The model for the integer quantum Hall states is relatively simple; in a $2d$ system of non-interacting fermions, apply a magnetic field perpendicular to the sample. The Hamiltonian for this system is $H = \frac{1}{2m}(\vec{p} + e\vec{A})^2$, and solving for the energy spectrum reveals a set of Landau energy levels which are highly degenerate.

The above Hamiltonian was first examined experimentally in an electron gas, where famously it was noted that the Hall conductance was quantized over extended values of the magnetic field strength to

$$\sigma_{xy} = \frac{I_{edge}}{V_{hall}} = \eta \frac{e^2}{2\pi},$$

where η is an integer counting the number of filled Landau levels. Additionally, the IQH systems exhibit chiral edge modes when the size of the sample is finite. These edge modes, which transport electric charge, are notably different from typical transport; in both the classical and quantum picture, one finds that electrons travel unobstructed along the edge. The charges will move around any impurity, and this transport property is what is referred to by the term chiral.

As it turns out, these edge modes cannot occur without the presence of the bulk, and along with the quantization of the Hall conductance, this signals something topological about the system. The topology of the system belongs to the band structure and is an effect of adiabatically taking the ground state of a given band around a closed loop in parameter space.

In particular, a clean $2d$ quantum Hall system on a torus has wavefunctions that can be written in terms of Bloch states:

$$\psi_{\vec{k}} = e^{i\vec{k}\cdot\vec{x}} u_{\vec{k}}(\vec{x})$$

where $u_{\vec{x}}$ is periodic in the length of the x or y directions. For these translationally invariant systems, $\vec{k}$ serves as a set of two good quantum numbers, k_x and k_y, that live on a torus $\boldsymbol{T}^2_{\vec{k}}$. Therefore, a band structure is well defined, and the Bloch state decomposition can be done for each band. In a single band, α, the Bloch states $u_{\vec{x}}$ are continuous, and the phase acquired between them winds

as one goes through the toroidal Brillouin zone. The Berry connection over the two momenta directions, defined as

$$\mathcal{A}_i(\vec{k}) = -i\langle u_{\vec{k}}|\frac{\partial}{\partial k^i}|u_{\vec{k}}\rangle,$$

allows us to probe the curvature of the space of states in the band.

By associating a field strength to this connection, $\mathcal{F}_{xy} = \frac{\partial \mathcal{A}_x}{\partial k^y} - \frac{\partial \mathcal{A}_y}{\partial k^x}$, we can compute a quantity that captures the topology of the band α, known as the Chern number:

$$C_\alpha = -\frac{1}{2\pi}\int_{\boldsymbol{T}^2_{\vec{k}}} d^2k\mathcal{F}_{xy}.$$

As it turns out, the Chern number is an integer, and the sum of C_α over all filled bands is precisely the integer appearing in the quantization of the Hall conductance. It is the topological invariant that is manifest in the IQH states; as an integer cannot change continuously, a distinct topological phase is seen for a given Chern number, $C = \sum_\alpha C_\alpha$, and the extended regions of quantization are those for which C remains unchanged.

For more generic and complex manifolds, where a band structure is not well defined, the Chern number can still be computed by defining a field strength over parameters of the Hamiltonian. A common trick is to imagine inserting a magnetic flux around each hole in the manifold, and the strength of the flux represents the Hamiltonian parameters. Because the system is periodic in the strength of the fluxes, integration around these closed loops will also produce the Chern number.

We conclude by again noting that the IQH states are thermal, and the effect is only well defined in the limit of zero temperature. While the effect is particularly illuminating to generic properties of topological phases, it does not represent the most recent frontier in condensed matter physics. For this purpose, we turn our attention to the physics of quantum systems driven far from equilibrium. We will need to develop new tools to describe these systems, and the physics of dynamical topological phases will change accordingly.

1.2 Thermalization and Many Body Localization

While the notion of equilibrium is well established for systems coupled to external reservoirs, as in integer quantum Hall systems, chiral Floquet phases occur solely in closed quantum systems. In

this regime, the physics and very definition of equilibrium differ from those developed in standard statistical mechanics and thermodynamics. This will require us to develop new tools for describing the behavior of closed systems

In particular, it is clear how an open (e.g. solid state) system equilibrates (thermalizes); through the exchange of heat between a system in good thermal contact with a reservoir, an equilibrium state will be reached where the system and reservoir are described by the same thermodynamic quantities. Note that such notions of equilibrium only become sharp in the thermodynamic limit, which represents a set of limits that must be taken. Namely, the size of the combined reservoir and system must be taken to infinity, followed by the time, and finally the size of the reservoir alone. The first and third limits are necessary because equilibrium is only well defined in infinite systems, while the infinite time limit is required to capture the growing time needed for a larger system to equilibrate.

In these quantum systems, equilibrium is best understood in terms of the density (probability) operator. Given a state $|\Psi\rangle$ of the entire system and reservoir, the density operator is defined as $\rho = |\Psi\rangle\langle\Psi|$. The utility of describing a state this way is evident when we wish to deal with mixed instead of pure states, which is always the case in equilibrium settings. Given that the system and its global environment have no information about any other system, then $|\Psi\rangle$ is known to be a pure state. If, on the other hand, we wish to describe the dynamics of a system (A) separate from the reservoir (B) then we may perform a partial trace over all of the states in B to get the reduced density matrix of A: $\rho_A = \mathrm{tr}_B(\rho)$. If the state of A depends to some extent on the state of B, then $|\Psi\rangle$ cannot be decomposed into a product state of the environment and the system. The density matrix formulation will capture this feature, and the dynamics of ρ_A follow the same rules as the total density matrix.

Given this construction, statistical mechanics predicts that the reduced density operator, ρ_A, of a quantum system in thermal equilibrium with a reservoir will have an expected equilibrium value of

$$\lim_{N_B\to\infty}\lim_{t\to\infty}\rho_A(t) = \rho^{(\mathrm{eq})}(T) \equiv \frac{1}{Z(T)}\exp(-H/k_BT) \tag{1.1}$$

where Z is the partition function. This density operator predicts the probability of finding the system in a particular microstate.

What happens, then, when one asks whether a closed quantum system reaches thermal equilib-

rium? The definition above no longer works, since there is no reservoir with which heat exchange can occur. Instead, imagine slicing our closed system into two subsystems, A and B. Thermalization in such quantum systems is defined as the ability of B to serve as a thermal reservoir for subsystem A in the thermodynamic limit.

This is a rather vague statement, however. To be more precise, the state of the system at any time is given by the density operator, ρ, defined above. Where energy is the sole conserved quantity, the equilibrium state of the system is described entirely by the temperature [19]. Moreover, the initial state possesses some non-zero energy density such that the system is out of equilibrium. If the closed quantum system is thermal, then the state of any subsystem A in the thermodynamic limit is one that is in thermal equilibrium with subsystem B (i.e. the temperature of A). This requires that the reduced density operator satisfy equation 1.1.

A subtle assumption in describing thermalizing systems is that if one system thermalizes for a given energy density, then all initial states with the same energy content will thermalize [19]. This assumption leads us directly to the Eigenstate Thermalization Hypothesis (ETH), which we take to be true for thermalizing systems.

A particularly useful measure of the information shared between quantum systems is in their entanglement entropies, and the way these quantities scale will tell us a great deal about whether or not a closed quantum system thermalizes. For example, one may consider a Schrodinger cat state of spin-1/2's of the form $|\psi\rangle = \frac{1}{\sqrt{2}} \left(|\uparrow_A\rangle |\downarrow_B\rangle + |\downarrow_A\rangle |\uparrow_B\rangle \right)$. It is impossible to factor this state into a product state of $|\psi_A\rangle$ and $|\psi_B\rangle$, and they are considered to be quantum entangled. To describe the dynamics of the state of spin A without worrying about spin B, we can construct the reduced density matrix for spin A. To quantify the extent at which the two states are entangled, we use the von Neumann entanglement entropy:

$$S(A) = -\text{tr}_A \left(\rho_A \log \rho_A \right) \tag{1.2}$$

For the particular example considered above, $S(A) = \log 2$. In open quantum systems, the nature of equilibrium arises from the states in the system being highly entangled with the reservoir. In closed quantum settings, this idea is still tenable; entangled states cannot be factored into product states of the two subsystems, and the extent to which this is true is a defining feature of thermal systems. Recall that thermalization means that the system is described by standard statis-

tical mechanical measures at equilibrium. Since the equilibrium value for the entropy of subsystem A scales with the volume of the subsystem, the thermalizing eigenstates have characteristic volume-law scaling of entanglement [19].

Perhaps the most striking result of the above analysis is that not all closed systems thermalize, and such systems are said to be localized. Broadly speaking, a system that is localized does not satisfy the condition of equation 1.1 [19]. It's not too difficult to think of a system that obviously violates this; it would be impossible for an isolated non-interacting system to thermalize. For example, consider a chain of spin-1/2's with any initial configuration, with a Hamiltonian

$$H = \sum_i h_i S_i^z$$

The spins are unable to interact with each other and are therefore unable to share information in a system under the dynamics of this Hamiltonian.

In this simple scenario, the eigenstates of the Hamiltonian's do not obey the Eigenstate Thermalization Hypothesis [19]. However, this is not the problem of interest to us. Instead, we wish to consider a quantum system of many particles and strong interactions, and whether or not these systems can be made to localize. If we consider an extension of the spin model suggested above to include interactions:

$$H = J \sum_i \vec{S}_i \cdot \vec{S}_{i+1} + h_i S_i^z \tag{1.3}$$

then it's clear that the $J = 0$ limit reproduces the many-particle non interacting localized system [19]. If the h_i are drawn from a uniform random distribution ($h_i \in [-h, h]$) then in the limit of weak interaction and strong disorder ($J \ll h$), perturbation theory [20] and strong numerical evidence [21–23] predicts that thermalization does not occur. In particular, the investigations in Ref. [20] show that to all orders of perturbation theory, the metal-insulator transition amplitude for an electronic state vanishes strongly, showing localization for weak interactions.

More strikingly, however, is that in the more extreme regime of $J \approx h$ (i.e. the strong interaction realm) the ETH persistently fails for this model [19]. These many body localized (MBL) phases have driven recent research in complex quantum systems and makes possible the realization of strongly interacting systems with the intriguing properties of the MBL regime [2–7].

In particular, there are a few key properties associated with many body localized systems that

differ from their thermal counterparts. First and foremost, local observables in these systems are found to store information about the initial conditions for arbitrarily long times [19]. Moreover, we saw that thermal systems exhibit volume-law scaling of their entanglement entropies. However, the single and multi-particle localized phases show a weaker area-law scaling [19]. This makes intuitive sense: the degrees of freedom in an MBL system are localized within a localization length, preventing long range entanglement. Lastly, the spreading of entanglement in MBL systems is characteristically slow compared to the power-law spread of entanglement in thermal systems [19]. More precisely, it is logarithmic in time [24, 25], a property that has been used in research reliant on MBL systems (Ref. [26], for example).

A utility of the MBL phase is that the localization allows us to rewrite the Hamiltonian of interest [19], and in a way that makes the above properties of MBL more transparent. While some systems exhibit MBL behavior in some (but not all) of their eigenstates, there are some systems which are considered fully many body localized [19]. These systems appear at sufficiently strong disorder, and the eigenstates of the Hamiltonian are all localized [19]. In particular, we may introduce local integrals of motion (l-bits), which are exponentially localized in real space, to describe the dynamics [24, 25, 27]. This follows intuitively form the fact that the many body states are locally spread over the physical degrees of freedom (p-bits) such that we might assume there exists some composite degree of freedom that describes the behavior of the localized state [19]. These l-bits represent, in some sense, a conserved quantity that doesn't change under the Hamiltonian dynamics [19].

In a fully many body localized system consisting of two state quantities, the l-bit's have their own Pauli operators, denoted by the set $\vec{\tau}_i$, and the Hamiltonian of this system can be written as [19]

$$H = E_0 + \sum_i \tau_i^z + \sum_{ij} J_{ij}\tau_i^z\tau_j^z + \sum_{n=1}^{\infty}\sum_{i,j,\{k\}} K^{(n)}_{i\{k\}j}\tau_i^z\tau_{k_1}^z\ldots\tau_{k_n}^z\tau_j^z$$

Let us consider the implications of the above Hamiltonian. First, note that E_0 is a constant, and the interaction strength of J and K decreases exponentially away from their support [19]. The absence of charge transport is characteristic of MBL systems, so it should make sense that the l-bits exist in the first place; they are conserved quantities of the system, and as such satisfy $[H, \vec{\tau}_i] = 0$ [19]. As a result, the eigenstates of the Hamiltonian are themselves the eigenstates of the l-bit Pauli operators, making the system particularly easy to analyze.

The key feature to notice is that if we think of the l-bits as spins, the above Hamiltonian contains no terms that actually flip a spin. Instead, the presence of only τ^z implies that the interaction terms between l-bits cause them to precess [19]. This is a powerful statement because it precisely captures the notion that MBL systems retain information about their state's initial conditions, which is due to the fact that dephasing is can in principle be undone to recover the information about the initial conditions [19].

Additionally, the l-bit picture predicts the log slow growth of entanglement. The effective interaction between terms J_{ij} and $K^{(n)}_{i\{k\}j}$ in the Hamiltonian

$$J^{eff} = J_{ij}\tau^z_i\tau^z_j + \sum_{n=1}^{\infty}\sum_{\{k\}} K^{(n)}_{i\{k\}j}\tau^z_i\tau^z_{k_1}\ldots\tau^z_{k_n}\tau^z_j$$

go exponentially ($\exp(_L/\xi)$) with distance between qubits for localized systems [19]. When the interaction terms of the Hamiltonian satisfy $J^{eff}t \leq 1$ then two qubits separated by a distance L will become entangled [19]. This condition implies the log-slow growth of entanglement in interacting MBL systems, namely $L \approx \xi \ln(J_0 t)$ [19].

It should be noted that while the thermal and MBL phases are distinct (and a system can in fact undergo a phase transition between these), it is not in the sense of phases of matter that we are typically familiar with [19]. Instead, the Eigenstate Thermalization Hypothesis allows us to predict the behavior of the eigenstates of a Hamiltonian and to determine whether or not the properties of these will be thermal [19]. In this regard, the eigenstates drive the dynamics of an MBL system which we're interested in [19].

1.3 Floquet MBL Systems

While the integer quantum Hall states have done a great deal in revealing the possibility of topological phases, advances in AMO and superconducting qubit systems have allowed for the possibility of realizing out-of-equilibrium phases. Moreover, theoretical efforts have indeed shown that topological systems exist in highly excited states. Of particular interest to this work are those excited states arising from periodic (Floquet) driving, and we will find that the results of many body localized states play an important part in the development of Floquet systems.

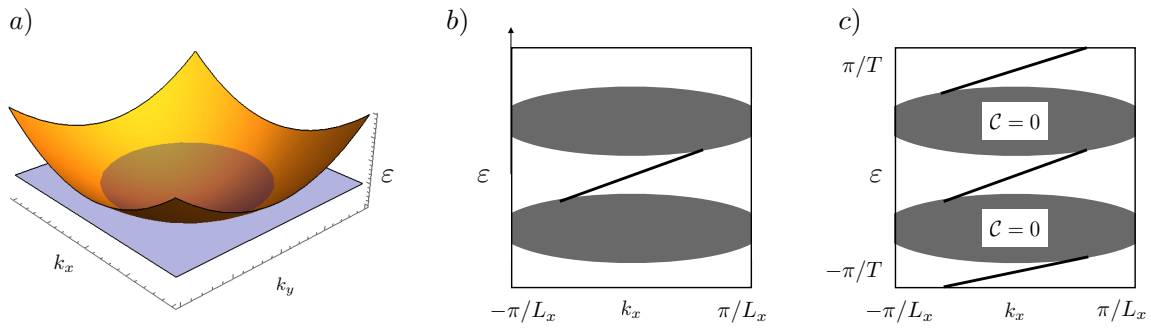

Figure 1.3.1: a) shows an example of a band structure for a $2d$ system with translational symmetry. b) shows the $2d$ band structure compressed into 1 dimension when a physical edge is opened pointing along k_x. This is done by intersecting the curve in (a) by a constant energy and mapping the k_y values to k_x, giving an extended region of bulk band structure (shaded region). In this case, the energy of the system is bounded, and the bulk bands can possess non-zero Chern number. This signals the presence of edge modes, which are shown by the independent lines crossing the band gap. c) shows the same band structure when the system is also Floquet; the energy becomes quasi-periodic, and the Chern number of the bulk bands is no longer sufficient in characterizing the presence of edge modes. Here, chiral edges are present, despite the Chern number (the difference of chiral states above and below the bulk bands) being zero.

In Floquet systems, we have a time dependent Hamiltonian satisfying $H(t+T) = H(t)$. One can define a Floquet unitary to be

$$U_F(T) = \mathcal{T}\{e^{-i\int_0^T H(t)dt}\}$$

which evolves the state of the system forward in time by one period. Here, $\mathcal{T}$ denotes a time ordering of the operators. This unitary takes the place of the traditional e^{-iHt} evolution in static systems.

The periodicity of Floquet systems endow them with a discrete translational symmetry in time, from which we may apply Floquet's Theorem. The eigenstates of the Floquet operator, $|\Psi\rangle$, may then be written as

$$|\Psi(t)\rangle = e^{-i\varepsilon t}|\Phi(t)\rangle$$

where $|\Phi(t)\rangle$ is periodic in the period of the drive. Moreover, the quantity ε is identified as a quasi-energy of the system. Because the Hamiltonian is time dependent, the notion of conserved energy

no longer exists. However, the quasi-energies allow for a useful tool in describing the states of these systems. It should be noted that the quasi-energy is only defined mod $2\pi/T$ since $|\Phi(t)\rangle$ can be modified by any time-periodic phase (i.e. it is not uniquely defined by this equation).

In translationally invariant non-interacting systems, analysis can be done in terms of their band structure. In Floquet systems with these same properties, it is still possible to associate a band structure to them, though the specifics are slightly modified. Suppose, for example, we have a $2d$ system that is subjected to Floquet dynamics that possesses translational symmetry, and the system is periodic in x and open in y. This opens two system edges, in the direction of the crystal momentum k_x along the edge. In two dimensions, the band structure might look like that in Fig. 1.3.1a. If we bisect the bands by some quasi energy value ε and project the crystal momenta k_y onto the k_x values for that energy, we can construct a $1d$ band structure as in Fig. 1.3.1c.

Upon doing this, it is possible that we find edge modes for certain quasi-energies. More precisely, a band structure that is topologically non-trivial will give rise to edge modes when a system edge is exposed. For such finite systems, there exist regions for which the band structure is the same as an infinite system; these regions are the bulk and are shaded in the band structures of Fig. 1.3.1b and c. Moreover, these sets of bands possess gaps. However, introducing edges to the system can reveal edge modes between the bulk gaps that are explicitly localized to the system edge due to the changes to the Hamiltonian in these cases.

If the system were not Floquet, the energy would be bounded and the edge modes can be characterized by the Chern number that we introduced above; this quantity has the simple interpretation of measuring the number of edge modes lying above or below the bulk band. For example, such a non-Floquet $1d$ band structure is depicted in Fig. 1.3.1b. If the chemical potential of the system sits in the band gap, we would find edge modes propagating with the corresponding wavenumber.

On the other hand, a Floquet systems possess different band structure properties. Because of the quasi-energies being periodic, the chemical potential is not well defined since the quasi-energies are not ordered. Due to these features of Floquet bands structures, it's possible for bulk bands to close and reopen around the periodic direction, revealing edge modes. Similar to the non-Floquet systems, these edge modes cannot be destroyed without closing the bulk bands again. However, the Chern number of the bulk can be zero (measuring the number of edge modes above and below the bands) in Floquet systems, despite the presence of edge modes, and it no longer characterizes the topology of the bands. We will explore the consequences of this in the next section

for a concrete example.

In Floquet settings, one might also wonder if the notion of many body localization is still tenable. After all, the entire analysis of thermalizing versus MBL systems was built on the properties of the Hamiltonian eigenstates. As it turns out, MBL can still be well defined in Floquet systems if we examine the eigenstates of the Floquet unitary [28]. However, the presence of disorder destroys the translational symmetry, and we will be unable to find an associated band structure as in Fig. 1.3.1. In the non-MBL context, it is possible to characterize the edge modes by the winding of the quasi-energies, whereas localization prevents such classifications. Despite this, edge modes will in fact exist, and we will be tasked with finding a way to identify these as topological properties of the bulk.

The motivation for studying Floquet MBL systems is in part due to studies that have shown that MBL systems can be stable in Floquet settings [28], which opens a host of possibilities. For one, MBL protects a system from drive induced heating [28–32]. Namely, a driven system will tend to absorb energy from the drive, leading to fast heating of the system. Many body localization prevents this from occurring. Equally important in this context is that Floquet MBL systems and their corresponding unitary can be written in terms of an effective time-independent Hamiltonian [28]. This Hamiltonian is quasi-local (with exponentially small weight on distance sites) in nature and is constructed in terms of local integrals of motion. The unitary then takes the form of a static Hamiltonian evolution [28]. These systems will play a crucial role in the development of chiral Floquet phases.

1.4 Chiral Floquet Phases

The out-of-equilibrium dynamics that are enabled by Floquet driving of MBL systems will become the central topic of the remainder of this work. In particular, we have now laid the foundation to introduce and study chiral Floquet phase models. These have been developed in the presence of anyonic excitations (quasi-particles having fractional quantum numbers) [7], but our discussion will focus primarily on those of interacting bosonic spins with p degrees of freedom each, as in [5]. To understand the importance of these bosonic models, it is enlightening to first consider the non-interacting fermion case, where CF phases were first developed [2–4].

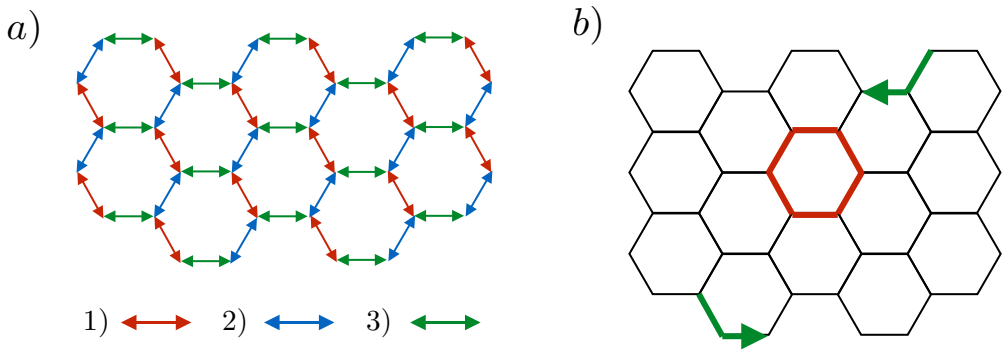

Figure 1.4.1: The non-interacting fermion chiral Floquet model is shown, with a driving protocol outlined in Ref. [2]. At each step of the drive, all legs of the hexagonal lattice have a hopping amplitude turned on. The color coding denotes which bonds have a hopping amplitude tuned to λJ. For example, at time step 1, the red bonds have a λJ hopping amplitude, while the blue and green bonds have an amplitude J. At time step 2, it is the blue bonds that have a λJ amplitude, and so on. In b) the net result of one period is shown schematically. Fermions at the edge (in green) of a sample propagate along the edge, while bulk fermions (in red) come back to where they started.

Consider the system shown in Fig. 1.4.1a. Each site of a hexagonal lattice is allowed to be occupied or unoccupied by a fermion. Given two sites connected along the x direction, the left most site is taken to be sub-lattice B whereas the rightmost is sub-lattice A. The tight binding model describing this system is of the following form

$$H = \sum_{\vec{k}} \begin{pmatrix} c^\dagger_{\vec{k},A} & c^\dagger_{\vec{k},B} \end{pmatrix} H(\vec{k}) \begin{pmatrix} c_{\vec{k},A} \\ c_{\vec{k},B} \end{pmatrix}$$
$$H(\vec{k}) = -\sum_i J_i(t)(\cos(\vec{b}_i \cdot \vec{k})\sigma_x + \sin(\vec{b}_i \cdot \vec{k})\sigma_y)$$

where $c^\dagger$ and c are the creation and annihilation operators of a fermion with crystal momentum $\vec{k}$ respectively. The lattice vectors, $\vec{b}_i$ are

$$\vec{b}_1 = (-1/2, \sqrt{3}/2) \qquad \vec{b}_2 = (-1/2, -\sqrt{3}/2) \qquad \vec{b}_3 = (1, 0)$$

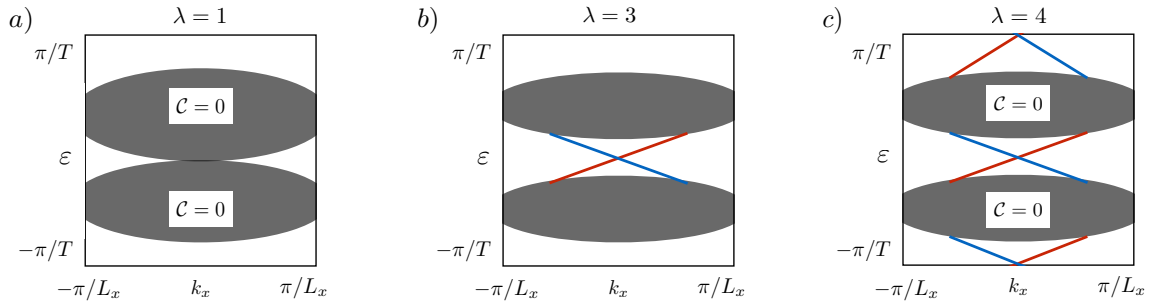

Figure 1.4.2: This diagram shows the wavevector, k_x, and the quasi-energy, ε, forming given band structures. The bulk bands are shown in grey and can be generic, complicated structures. The interesting characteristic is in the edge modes, with left/right propagating modes shown in blue/red. In a) for the $\lambda = 1$ parameter in the Hamiltonian, there is no bulk gap around $\varepsilon = 0$. In b) we have $\lambda = 3$, and the $\varepsilon = 0$ gap has opened, exposing two edge modes. Additionally, c) shows the band structure when the gap between the π/T and $-\pi/T$ quasi-energies has closed and reopened, revealing additional edge modes. The bulk bands with zero Chern number are also labeled.

A three step driving process is achieved by changing the hopping amplitudes as follows:

$$J_1 = \lambda J;\ J_2, J_3 = J \text{ when } nT < t \leq nT + T/3$$
$$J_2 = \lambda J;\ J_1, J_3 = J \text{ when } nT + T/3 < t \leq nT + 2T/3$$
$$J_3 = \lambda J;\ J_1, J_2 = J \text{ when } nT + 2T/3 < t \leq nT + T$$

When edges are exposed in the sample, chiral edge modes appear as in Fig. 1.4.1b. On the other hand, the bulk fermion states cycle back to their initial position after a driving period.

For different values of λ, one can examine the band structure when an edge is exposed along k_x, as in Fig. 1.4.2. Between $\lambda = 3$ and $\lambda = 4$, the band gap around quasi-energy 0 closes and reopens, exposing new edge modes. The bulk bands are then characterized by zero Chern number, despite the topological presence of the edge modes. As we expected would happen, the Floquet system is not well described by a Chern number, as the integer quantum Hall systems were.

These phases are our first real example that the Chern number is insufficient in classifying periodically driven topological phases. While a sufficient characterization of the different topological phases has been established in terms of winding numbers [2–4], it is unclear if this classification remains robust in the presence of interactions. Given the inherent imperfections in experimentally

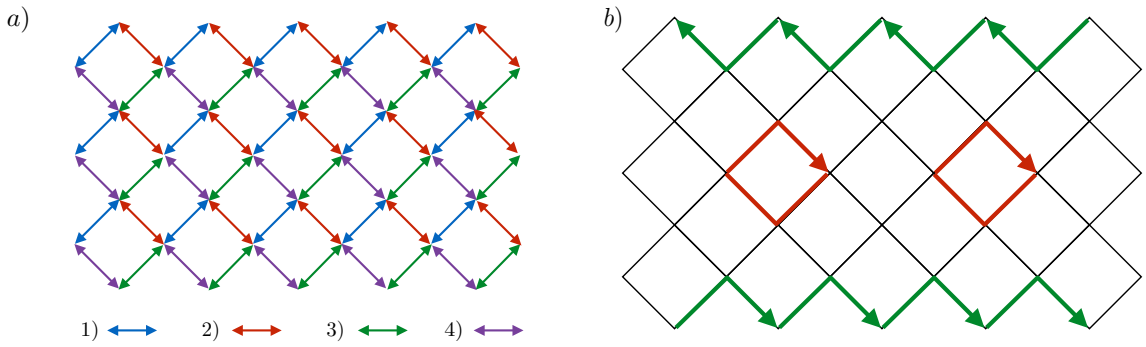

Figure 1.4.3: Periodic driving of a spin-1/2 system is shown schematically with the driving protocol outlined in Ref. [5]. Ideally, with no interactions, the SWAP model is achieved by permuting states at adjacent sites in four steps, the steps of which are color coded. The net result over one period is the edge states are transferred by one lattice site while the bulk evolution is trivial (the states return to their original position).

isolating systems and manipulating them, it would be compelling to identify chiral Floquet models that possess persistent edge modes when interactions are allowed and to determine how to classify them.

The model introduced in Ref. [5] sets the landscape for interacting Floquet systems, and it is shown schematically in Fig. 1.4.3b. Here, interactions are assumed to be absent for the time being. This ideal model periodically drives the states of the spins in a four step manner, where each step permutes the states of the appropriate sites. Evidently, this driving procedure brings the bulk states back to their position before the drive, but the edge states are transferred along the edge in a quantized amount. Without loss of generality, let us suppose we have a system of spin-1/2's. At each time step $\alpha = 1, 2, 3, 4$, we can write a Hamiltonian H_α that acts in a time $(\alpha - 1)T/4 \leq t \leq \alpha T/4$ as in [5]:

$$H_\alpha = \frac{\pi}{T} \sum_{\vec{r}} \left(\vec{S}_{\vec{r}_B + \vec{b}_\alpha} \cdot \vec{S}_{\vec{r}_A} - \mathbb{I} \right) \tag{1.4}$$

Here, $\vec{r}$ labels the location of a two site unit cell, with one site, A, having a basis vector of $\vec{0}$ from $\vec{r}$, and the other site, B, having basis vector $(\hat{x} + \hat{y})/2$. Note that $\hat{x}$ and $\hat{y}$ are unit vectors in their respective direction. The constants $\vec{b}_\alpha$ are given by

$$\vec{b}_1 = \vec{0} \qquad \vec{b}_2 = -\hat{x} \qquad \vec{b}_3 = -\hat{x} - \hat{y} \qquad \vec{b}_4 = -\hat{y}$$

The commuting terms in the Hamiltonian allow one to write a time evolution over time $T/4$ as [5]

$$U_\alpha \equiv \exp\left(-iH_\alpha T/4\right) = \prod_{\vec{r}} \frac{1}{2}\left(\mathbb{I} + 2\vec{S}_{\vec{r}_B+\vec{b}_\alpha} \cdot \vec{S}_{\vec{r}_A}\right)$$

Since each bulk spin returns to its original state after one period, $U_F = 1$ in the bulk. However, the striking property of the CF phase is that the edge dynamics are not so simple. In particular, consider the case of periodic boundary conditions along one direction, but open boundary conditions along the other. This gives rise to hard edges that feature translational motion of the spin states.

Mathematically, the four step permutation of the drive on the edge states consists of only two non-trivial steps (in the example above it is the third and fourth steps of the drive that are omitted) which can be represented by a translation operator that moves states to the left by one site [5]. Clearly, then, the Floquet operator at the edge differs from the bulk, and we may explicitly write the total Floquet operator as a tensor product of commuting operators, namely the identity on the bulk and a $1d$ translation operator on the edge [5]. This translation operators shifts each state on the edge by one lattice site.

In the presence of interactions, a many body localized bulk ensures that the decoupling of bulk and boundary evolutions is generic. In particular, one can introduce disorder (such as random magnetic fields) to produce an MBL bulk. The resulting bulk-boundary correspondence is notably different from non-Floquet settings, where an excitation gap and ground state allow for bulk phases to be distinguished from the boundary. Here, we suppose that our Floquet unitary is MBL (i.e. can be written in terms of l-bits). This is an essential ingredient, as more generic CF systems depend on the bulk being many body localized when interactions are allowed. Without this, the thermal bulk would leak quickly into the edge and spoil the edge modes.

Now, because of the exponentially well localized support for each operator, we can write the Floquet unitary as $U_F = \prod_r U_r$ for operators localized around the point r by a localization length, ξ. In a region (suppose it is a disk) R of the lattice, we can evolve the system in one of two ways; we can restrict the Hamiltonian to be a sum of local terms with support only in R: $H_R = \sum_{r:b(r)\subset R} H_r$ where $b(r)$ is a ball centered on r with a radius equal to the localization

length. Then, the Floquet unitary takes the form

$$U_F^1 = \mathcal{T}\Big\{\exp\left(-i\int_0^T dt H_R(t)\right)\Big\}.$$

Alternatively, we may just write the Floquet unitary as before, $U_F^2 = \prod_{r:b(r)\subset R} U_r$.

The second Floquet unitary, U_F^2, assumes the bulk is MBL, while the first unitary does not. If the two were the same, they would satisfy $(U_F^2)^{-1}U_F^1 = \mathbb{I}$. While this is exactly true in the bulk, it fails near the edge giving an effective edge unitary: $U_{edge} = (U_F^2)^{-1}U_F^1$. If the unitaries are exponentially localized with localization length ξ, then this sets the maximum distance with which two points in the ball $b(r)$ can communicate. The effective edge unitary is then localized to a distance ξ from the edge of the region R.

Strikingly, the edge modes persist when interactions between the bosons are turned on, provided the system is many body localized. As it turns out, the separation of the Floquet operator into commuting bulk and edge pieces is still possible in the presence of these more generic interactions, the difference being that the edge becomes an exponentially localized quasi-$1d$ strip with Floquet unitary evolution $U_{1d} = e^{-iH_{1d}T}\tau$ [5]. Here, the $1d$ Hamiltonian H_{1d} represents the effective interactions acting on the quasi-$1d$ strip, while τ translates all edge states by one lattice site. This follows immediately from the above considerations; the MBL bulk is robust against perturbations and physical deformations to the Hamiltonian. So long as the MBL is not disrupted, the two Floquet operators considered above still cancel exactly in the bulk, and the effective edge unitaries stay the same.

Unlike the non-interacting fermion model, the interacting bosonic spin CF phases do not have a well defined band structure. This is due to the presence of interactions and the MBL bulk which break translational invariance, and band structure is no longer defined. Therefore, band structure cannot be used to analyze CF phases, and the Chern number, even in its more general constructions, does not suffice in distinguishing different topological CF phases. Moreover, the winding number characterization for the non-interacting fermion models may not be robust to interactions. To formally classify each phase, then, one can introduce a topological invariant, ν, called the chiral unitary index [5]. This construction will capture the edge dynamics by quantifying the amount of quantum information being transferred along the systems edge.

To begin, take the effective $1d$ edge of our system and imagine cutting it into two sides, left

(L) and right (R). On each site, there exists a basis set of local operators. Because all operators acting solely on one site can be constructed in terms of this basis, they are closed under addition and multiplication, forming an operator algebra (the set of all local operators for that site). By extension, an operator algebra can be defined on a collection of sites, in this case the left and right sides of the $1d$ edge.

The basis for the states in each region, $\{|i\rangle\}$, endow the algebra with a basis of orthonormal matrices: $e_{ij} = |i\rangle\langle j|$. The orthonormality of the operators is defined in terms of the operator inner product, given by

$$\langle \mathcal{O}_1, \mathcal{O}_2 \rangle = \text{tr}\left(\mathcal{O}_1^\dagger \mathcal{O}_2\right)$$

tracing over all states in the region encompassed by the algebra. By extension, the extent to which two algebras are independent is given by [5]:

$$\langle \mathcal{A}, \mathcal{B} \rangle \equiv \frac{\sqrt{D_A D_B}}{D_{A\cup B}} \sqrt{\sum_{i,j=1}^{D_A} \sum_{k,l=1}^{D_B} |\langle e_{ij}^{(A)}, e_{kl}^{(B)} \rangle|^2} \tag{1.5}$$

where D is the dimension of the Hilbert space of the regions of the respective algebras. This quantity is 1 if the algebras are commuting (they share no information) and D_A if $\mathcal{A} = \mathcal{B}$. If we time evolve the left algebra over a period and take the inner product with the right algebra, this will measure the amount of information that has transferred to the right of the system. The opposite can be done, where the right algebra is evolved, and the ratios of these quantities will be a rational number. The chiral unitary index is defined as [5]

$$\nu \equiv \frac{\langle U^\dagger \mathcal{A}_L U, \mathcal{A}_R \rangle}{\langle \mathcal{A}_L, U^\dagger \mathcal{A}_R U \rangle} \tag{1.6}$$

and this serves as the topological invariant to characterize the edge modes of a CF phase. For a system of spin-1/2's, it takes the value of $\log 2$. In the next section, we will explore the limitations of this invariant and introduce a quantity that overcomes the drawbacks of ν.

2

Chiral Mutual Information

The classification of chiral Floquet phases has been, until now, reliant upon the chiral unitary index. The definition presented for the chiral unitary index works well for theoretical work, but a sense of physical intuitition is lost in the process. The physical transfer of quantum states is not well captured by the notion of algebraic overlaps, and in this sense the chiral unitary index is insufficient.

Moreover, the utility of chiral Floquet phases in future quantum devices lies primarily in the ability to transfer quantum states in a quantized, fault tolerant manner. Progress in understanding the behavior of CF phases in finite size, real world systems is entirely dependent on ones ability to experimentally characterize the edge modes. To this end, the chiral unitary invariant fails; while it is a powerful theoretical tool, measuring it would be, in practice, far too complex.

In light of these drawbacks, we proceed to define an alternative quantity to characterize the chiral edges of a CF phase. Working in terms of entanglement entropy measures, we find that it is possible to construct a quantity that is more physically transparent and could be measured in an experimental setting. Advances in AMO physics and superconducting qubit array construction

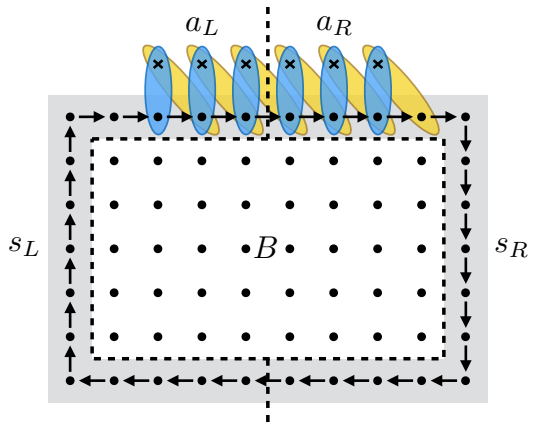

Figure 2.1.1: The ancilla-system entanglement scheme for an effective $1d$ CF edge. The effective edge is shown in grey. The entanglement bonds prior to a period of evolution is in blue, while the entanglement bonds after a period are shown in yellow. The left/right sides of the ancilla are labeled by $a_{L/R}$ (similarly for the system spins) and the bulk is labeled by B.

have made this a reasonable goal to seek, and we will propose a candidate experimental scheme for implementing our new edge characterization.

2.1 Quantifying CF Phase Edge Dynamics

Recall that physically it is quantum states being transported by the chiral edges, and that this quantum information is *not* carried by a measurable conserved current. In a chiral Floquet system, we do not have access to physically measurable quantities to distinguish different phases, as in the quantum Hall case. This property makes characterizing the edge dynamics particularly difficult. To track this motion of quantum states, however, we can appeal to measures of entanglement entropy on the chiral edges.

Suppose each site of a chiral Floquet system hosts a spin-$1/2$. The ensuing analysis will generalize to any higher number of degrees of freedom, though we choose spin-$1/2$ for simplicity. Consider, then, introducing non-dynamical ancillary spins to track the motion of the chiral edge. Prepare each ancilla in a maximally entangled state with its neighboring system spin. If we make an imaginary cut at the edge of our system, a single Floquet period will shift an entanglement bond across this cut (see Fig. 2.1.1). It is generally necessary to extend the region of ancilla coverage

into the bulk to capture all motion within a few localization lengths of the edge (this feature is suppressed in Fig. 2.1.1). This is to ensure any interactions between the edge and bulk are tracked.

With this physical construction, we consider a difference in mutual information between the left ancilla and right system spins versus the opposite pairing of right ancilla and left system spins. Introducing the chiral mutual information (χMI), it takes the form

$$\chi = \mathcal{I}(a_L, s_R) - \mathcal{I}(a_R, s_L) \tag{2.1}$$

where $\mathcal{I}(A, B) = [s(A) + S(B) - S(A \cup B)]/2$ and the von Neumann entropies are $S(A) = -\text{tr}(\rho_A \log \rho_A)$. This quantity is to be measured after a Floquet period.

The benefit of this construction is two-fold; not only is the χMI transparent in its interpretation of the edge dynamics, but it can be equally well defined by replacing the von Nuemann entropies with Renyi entropies, which can be measured experimentally with interferometric techniques [17, 18]. This prospect is a leading motivation for considering this alternative formulation of the topological invariant, and its exact behavior will be the topic of the remainder of this work.

2.2 Analytic Proof of Quantization

One cannot, in practice, ignore the effects of the bulk evolution. Although the edge evolution can be described by a local unitary operator that is independent from the bulk, the presence of the bulk spoils the simple picture that the chiral mutual information has afforded us. In particular, the edge and bulk formally factorize in the l-bit description, but in practice we do not know how to draw the dividing line in a given system, and need to consider the bulk evolution. With careful considerations, however, the quantification of quantum information transfer in terms of the χMI can be recovered.

Let us first establish a proof that the χMI is a topological invariant of a chiral Floquet phase with a frozen bulk. In this limit, we may first and foremost simplify χ. Recall that χ is defined as

$$\chi = I(a_L, s_R) - I(a_R, s_L)$$

where the letters a, s denote the ancilla and system, and the subscripts R, L denote the left or right

side of the imaginary cut. If we expand this out, we have

$$\chi = \frac{1}{2}\Big[S(s_L) - S(s_R) + S(a_L) - S(a_R) + S(a_L \cup s_R) - S(a_R \cup s_L)\Big]$$

Because the ancilla are non-dynamical, $S(a_L) = S(a_R)$, as long as there are equal numbers of ancilla on the left and right side of the cut, so these cancel out. Moreover, $S(a_L \cup s_R) = S(a_R \cup s_L)$ by complementarity, and therefore

$$\chi = \frac{1}{2}\Big[S(s_L) - S(s_R)\Big] \tag{2.2}$$

where, as before, $S(A) = -\text{tr}(\rho_A \log \rho_A)$.

In a pure translational evolution, i.e. with Floquet operator $U = e^{-iHt}\tau$ and $t = 0$, the model of Fig. 2.1.1 shifts one entanglement bond from the left to the right. If initially there were $N_a/2$ entanglement bonds on each side of the cut, then after a translation $S(s_R) = (N_a/2 + 1)\log 2$ and $S(s_L) = (N_a/2 - 1)\log 2$. Evidently, $\chi = \log 2$ for pure translation and the χMI reproduces the chiral unitary index.

If we instead include some $1d$ evolution, we can consider the effects of the e^{-iHt} part of the evolution by decomposing it into infinitesimal steps. First, the local structure of the Hamiltonian means we may break it into left/right (L/R) pieces that do not act near the cut, and a piece V that has local support on both sides of the cut. Now, consider the step from some t_0 to $t_0 + \Delta t$. In the limit that $\Delta t \to 0$, we may say that $U(t_0 + \Delta t) \approx U(t_0)\left(U_L U_R e^{-iV\Delta t} + \mathcal{O}(\Delta t^2)\right)$. The term $U_L U_R$ does not act near the cut, so we are left to show that $e^{-iV\Delta t}$ does not contribute to χ.

In the limit that $L, N_a \to \infty$, then the finite speed of information transfer (the bound of which is set by the Lieb-Robinson velocity [33]) guarantees that unentangled system spins will not leak into the ancilla region near the cut. If the ancilla entanglement is maximal with the spins, we may evolve the ancilla instead of the system spins by U_V^T. However, such an evolution doesn't change the overall entanglement of the left or right sides of the system (such that $\partial S(s_{L/R})/\partial t = 0$) for which the χMI has been reduced to. This immediately implies that $\partial\chi/\partial t = 0$. This ensures that χ is a topological invariant (unaffected by local perturbations), and in the $L, N_a \to \infty$ limit with no bulk interactions, may be used to replace the chiral unitary index.

Note that this proof requires that the ancilla be maximally entangled with the physical spins.

However, we've previously seen that uniform partial entanglement seems to be able to reproduce the chiral mutual information as well (see Fig. 2.4.2). It is presently unclear how this construction (away from maximal entanglement) would hold up when the bulk interactions are considered.

At what point does our construction of the chiral mutual information break down? In finite size systems for which the bulk motion has been frozen, we observed that the chiral mutual information is precisely quantized up to the Lieb-Robinson bound, which arose from the influence of system spins not being tracked by ancilla crossing the cut. In theory and in practice, we could simply take the limit of large system and ancillary spins to achieve precise quantization for arbitrary times. When the bulk is allowed to evolve, however, the spins will immediately begin to entangle with the edge states, and this will contribute a net flow of information that is unaccounted for in the definition of the chiral mutual information.

This issue can be addressed by extending the region of ancilla coverage into the bulk by a few localization lengths, ξ. While such a construction captures the chiral motion we wish to characterize, other non-topological interactions need to be considered. Broadly speaking, entanglement can be generated between spins from the ancilla covered and non-ancilla regions, or the spins can undergo a complete state swap. For the chiral mutual information to remain a satisfactory characterization of the edge dynamics, we will require that these interactions do not contribute to χ or that their effects can be extracted from the true chiral motion. Note that interaction that are restricted to a single subregion of our configuration (i.e. s_L, a_L, etc.) do not change the chiral mutual information. This is evident since interactions within s_L, for example, do not change the corresponding entanglement entropy $S(s_L)$ that the region has with the rest of the system.

Consider first the interaction between two neighboring system spins, in the region covered by ancilla, on the left and right side of the cut. If the states of these spins are swapped, we can show that this does not contribute to χ. Recall that by our definition, we may write

$$\chi = \Big(S(a_L) - S(a_R)\Big) + \Big(S(s_R) - S(s_L)\Big) + \Big(S(a_R \cup s_L) - S(a_L \cup s_R)\Big)$$

Now suppose there are N_a ancilla on the right side of the cut and N_s sites on the left side of the cut. If the configuration is prepared in a state with the system spins maximally entangled with their ancillary counterpart, then initially $S(a_R \cup s_L)$ shares $N_a + N_s$ entanglement bonds with everything else. Upon swapping the states of the two spins, and in the absence of any other

interactions, there is a single spin in a_R and a single spin in s_L that are entangled with one another, but not with anything outside of the region $a_R \cup s_L$. Therefore, the quantity $S(a_R \cup s_L)$ loses two entanglement bonds. However, the effect of this swap on $S(a_L \cup s_R)$ is identical. All other terms are unchanged. Since $S(a_R \cup s_L)$ and $S(a_L \cup s_R)$ are otherwise equal, and they appear with opposite signs, this contribution cancels, leaving χ invariant to such interactions.

Alternatively, consider the interactions between a neighboring bulk and system spin (at the boundary of ancilla entanglement) further than a localization length, ξ, away from the triple intersection of the bulk and left/right sides of the system. Suppose we look at spins in the region s_L. If there are N_s spins contained in this region, then $S(s_L)$ initially corresponds to N_s entanglement bonds. If these two spins are swapped, this reduces the number of entanglement bonds of s_L with the rest of the configuration by one since we are not tracking the bulk spins (the new state occupying the site is not entangled with anything, whereas the initial state was entangled with an ancilla). Similarly, the region $a_R \cup s_L$ loses an entanglement bond with the rest of the configuration. Appealing to our definition of χ, $S(s_L)$ and $S(a_R \cup s_L)$ appear with opposite signs, so their contributions to χ cancel, leaving our quantity invariant.

If, on the other hand, the two neighboring spins become entangled, there remains no change to the terms in χ. $S(s_L)$ does not change because the affected spin was initially maximally entangled and remains so (expect with different spins), and the same argument applies to $S(a_L)$. By the same line of reasoning, $S(a_R \cup s_L)$ is unchanged and χ is invariant to such interactions. Note that entanglement can continue to spread through the ancilla region until it reaches the chiral edge. However, since the ancilla reach into the bulk, entanglement spreads logarithmically slowly due to the MBL nature of the bulk. This point will be addressed shortly

The last non-topological interaction we should consider is a three-spin state interaction near the triple intersection of the uncovered bulk and the left/right sides of the system. At this point, a three-spin swap that transfers a bulk spin across the cut will appear chiral to the χMI. However, these bulk interactions occur logarithmically slowly in the MBL bulk.

Coupled with the log slow growth of entanglement from the bulk leaking towards the edge, there is a net contribution to χ that is non-topological. To account for this in practice, the system can be evolved over multiple periods, n. The true chiral motion will lead to a linear accumulation of entanglement crossing the cut equal to $n \log 2$. On the other hand, the non-topological contributions are restricted to $\chi_{\text{bulk}} \lesssim \log nT$ for a period T drive. The topological chiral contribution

can be recovered by finding $\lim_{n\to\infty} \chi(nT)/n$.

2.3 A Numerical Model for χMI

There are a number of challenges associated with the physical implementation of the chiral mutual information. For one, the above analysis relied on taking an infinite system size limit. However, a simplified numerical investigation provides meaningful insight towards the utility of the chiral mutual information for finite size systems. As a computational simplification, we suppose that we have a chiral Floquet phase for which we have frozen the bulk degrees of freedom. In this limit, we can treat the edge of our CF phase as an effectively 1D edge with periodic boundary conditions. We use ancilla to track the edge degrees of freedom only so that only a $1d$ chain of ancilla are necessary.

As usual, consider a chiral Floquet phase of L spin-1/2's, but now imagine that we're only concerned with a $1d$ edge. Moreover, we will track the information flow of these spins with N ancilla by making an imaginary cut of our $1d$ chain directly in the middle and placing equal numbers of ancilla on either side. Note that while there can be a different number of ancilla on either side of the cut, this must be accounted for in the transfer of information in χ, so we do not address this case. We will also suppose, for simplicity, that L is even. We will work with the case that $N < L$. Because we have periodic boundary conditions, working with $N = L$ would result in equal amounts of information flowing into the left half and the right half of the system which would cancel each other out. In this section, we will appeal to the simplified version of χ that holds for a frozen bulk: $\chi = \frac{1}{2}\Big[S(s_L) - S(s_R)\Big]$.

To numerically model this scheme, an understanding of computational techniques must be developed. That is, how do we go between an analytical language and a numerical language as it applies to spin systems? In analytical settings, we typically do not write down every state in our Hilbert space (for larger systems this would take far too long). However, we must tell a computer very explicitly how to carry out problems in quantum mechanics which necessitates a thorough consideration of what the state vectors in our Hilbert space are and how operators act on them. While a great deal of this treatment is made in other works, let us expand on those ideas in the context of the present problem for clarity [34].

Each spin is a 2 state system, and from a numerical standpoint it is therefore useful to identify the spin states of our system with binary numbers. In particular, let a spin down be denoted by a 0

in our code, and a spin up by a 1. The state of our 1D system is then best represented by an array of 1's and 0's. For example, we could create a state array of $L = 10$ spins with a corresponding spin representation as

$$\text{state} = [0,1,1,0,1,1,1,0,0,1] \quad \text{is equivalent to} \quad \downarrow\uparrow\uparrow\downarrow\uparrow\uparrow\uparrow\downarrow\downarrow\uparrow$$

With such a representation for a spin system, how can we turn this into a vector that actually represents the state and can be acted upon? Moreover, we should now keep track of all the possible spin states that comprise our Hilbert space as well as construct all of the state vectors for operators to act on. For the $L = 10$ spin case, we know from basic probability that there should be 2^L spin states, so we conclude that any state vector will have 2^L elements. The simplest way to keep track of these states is to label the binary array of spins by their corresponding decimal value. For example, the above state in binary is 0110111001 which, in base 10, has a value of 441. Then, the corresponding state vector will be an array, indexed from 0 to $2^L - 1$, of all 0's with a 1 in the index representing a particular binary spin configuration. In this way, a spin state with all down spins should be a vector with a 1 in the 0 index position and zeros elsewhere, while a spin state with a spin up in the rightmost spot should be a vector with a 1 in the index 1 position and zeros elsewhere, and so on. An array of all of all such vectors will comprise our Hilbert space.

With state vectors for our spin configurations in hand, we turn our attention to the numerical construction of various operators that will be needed to act on these state vectors. The first one that we consider is the translation operator, τ. The construction of this is rather straightforward, as its effect is simply to translate each spin to the right by one site. Thus, a state array of the form $[0, 1, 1, 0, 1, 1, 1, 0, 0, 1]$ should be taken to

$$[0, 1, 1, 0, 1, 1, 1, 0, 0, 1] \rightarrow [1, 0, 1, 1, 0, 1, 1, 1, 0, 0]$$

Numerically, this operation can be achieved by performing a bit shift to the right on the binary number, then changing the leftmost number in the sequence (a bit shift will automatically put a 0 in this spot, so we must change this to a 1 if the rightmost number was a 1). To create a matrix that can act on the state vectors themselves (as opposed to the binary arrays), we can create a matrix, τ, of size $2^L \times 2^L$. For each state vector in our Hilbert space, i, we can find the binary representation

of the index, perform the translation above, then find the new corresponding decimal value of the binary state, j. Doing this for each state i in our space, the translation matrix should take values of $\tau(j,i) = 1$ in this indices, and zero elsewhere.

The other essential ingredient to numerically evolving our state vectors is a Hamiltonian. While the scheme for the chiral mutual information suggests any local Hamiltonian should be sufficient, we consider for concreteness a Hamiltonian with Heisenberg type interactions and a symmetry breaking term:

$$H_{1d} = \sum_{i=0}^{L-1} \left(J\vec{S}_i \cdot \vec{S}_{i+1} + h_i^z S_i^z + h_i^x S_i^x \right) \tag{2.3}$$

Here, $\vec{S}_i = \frac{1}{2}\vec{\sigma}_i$ and the terms $h_i^{x/z}$ represent random onsite potentials at each site of the lattice. The J term represents interactions between nearest neighbors, while the $h^{x/z}$ onsite potentials are included to break all symmetries and ensure that the model is non-integrable.

2.3.1 Constructing a $1d$ Hamiltonian

We must now tackle the challenge of constructing the Hamiltonian numerically. Let the $\mathbb{Z}_2$ symmetric portion of the Hamiltonian be denoted by $H_{1d}^{\mathbb{Z}}$ and the symmetry breaking term by H_{1d}^{SB}. The construction of the symmetry breaking operator can be understood in the following way. Recall that $S_i^x = \frac{1}{2}\Big(|\uparrow\rangle_i\langle\downarrow|_i + |\downarrow\rangle_i\langle\uparrow|_i \Big)$ where i indexes the sites of our system and there is an implicit tensor product with the identity at all other sites. To construct H_{1d}^{SB}, then, we should find the matrix representation of S_i^x for all i so that the matrix elements of this part of the Hamiltonian will be

$$H_{i,j}^{SB} = \sum_{k=0}^{L-1} h_k^x S_{k,(i,j)}^x$$

where k indexes the L sites of the system, and i, j run over all state vectors.

To find $S_{k,(i,j)}^x$ numerically, we should take the state vector $|j\rangle$ and determine its corresponding binary spin state. Then, we should flip the values of the spins at site k and determine the location of the resulting state in our Hilbert space. The decimal value of the resulting binary, i, will tell us that the component $S_{k,(i,j)}^x = \frac{1}{2}$. If this is carried out for each vector in the Hilbert space, we will have successfully constructed $S_{k,(i,j)}^x = \frac{1}{2}$. Doing this for all k gives us H_{1d}^{SB}.

We must also determine what the operator $H_{1d}^{\mathbb{Z}}$ will look like numerically. It is easiest to rewrite

the Hamiltonian as

$$H_{1d}^{\mathbb{Z}} = \sum_{k=0}^{L-1} \left(J\vec{S}_k \cdot \vec{S}_{k+1} + h_k^z S_k^z \right) = \sum_{k=1}^{L-1} J\left[S_k^z S_{k+1}^z + \frac{1}{2}\left(S_k^+ S_{k+1}^- + S_k^- S_{k+1}^+ \right) \right] + h_k^z S_k^z$$

where we have expressed S_k^x and S_k^y in terms of raising and lowering operators. To find the elements $H_{i,j}^{\mathbb{Z}}$, we will loop through all vectors in the Hilbert space, i, and consider the action of the Hamiltonian on them. Start by considering the diagonal components. The raising and lowering operators cannot connect two states for which $i = j$, and therefore do not contribute to these terms. Working in the S^z basis, a spin-1/2 has S^z eigenvalues of $\pm\frac{1}{2}$ so that the term $\langle i|S_k^z S_{k+1}^z|i\rangle$ takes the value $+\frac{1}{4}$ if the spins at sites k and $k+1$ are in the same direction, and $-\frac{1}{4}$ otherwise. Similarly, the term $\langle i|h_k^z S_k^z|i\rangle$ gives $\pm\frac{h_i^z}{2}$ for a spin up/down. We may loop through all Hilbert space vectors, i, and for each we should consider the binary state of spins it represents. By summing over all sites for each state, we can add the terms from above to find each diagonal component of $H_{1d}^{\mathbb{Z}}$.

For the off diagonal terms for which $i \neq j$, only $\langle i|\left(S_k^+ S_{k+1}^- + S_k^- S_{k+1}^+ \right)|j\rangle$ contributes. For this portion of the Hamiltonian, we should loop through all state vectors, i, and for each we should loop over the states and apply the raising or lowering operator. This amounts to finding the binary spin state corresponding to the vector i, flipping the spin at site $k+1$, and finding the resulting state in the Hilbert space, j, corresponding to the resulting binary spin state. Then, we know we should add $\frac{J}{2}$ to the off-diagonal term $H_{i,j}^{\mathbb{Z}}$ in the Hamiltonian.

2.3.2 Initial State Preparation

Having pieced together the terms for the Hamiltonian, we are prepared to proceed to the evolution of our state. Let us initialize the system spins in a configuration where the system spins that are unentangled with ancilla are pointing up, and those that are entangled exist in the state

$$|\psi\rangle = \cos(\alpha)|\uparrow\rangle_s|\downarrow\rangle_a - \sin(\alpha)|\downarrow\rangle_s|\uparrow\rangle_a$$

where s denotes the system and a denotes the ancilla. The α parameter allows for the adjustment of how entangled the ancilla are with the system. If we take a moment to consider the structure of our state, we know that the total state of the system and ancilla will be a tensor product of the states

of the spins at each site:

$$|\Psi\rangle = \prod_{i=0}^{L-1} |\psi\rangle_i$$

Since the ancilla are non-dynamical, we will ultimately be interested in the reduced density matrix for the system, namely $\rho_s = \sum_{i=0}^{2^N-1} \langle i|\Psi\rangle\langle\Psi|i\rangle$ where i indexes the states in the ancilla Hilbert space. To proceed, we will need to determine the state $|\Psi\rangle$ and perform the partial trace.

By careful observation, we note that by arranging the entanglement in the way that we have, we guarantee that our state $|\Psi\rangle$ can be written as a sum over all states in the Hilbert space of ancilla:

$$|\Psi\rangle = \sum_i c_i |\psi_s\rangle_i \otimes |\psi_a\rangle_i$$

where i now indexes all states in the ancilla Hilbert space, c_i are some constants, and $|\psi_s\rangle$ represents the system spin configuration for each particular ancilla configuration. By this we mean that if we consider a particular configuration of ancilla spins, say all down, then by the way we've entangled them we know that the corresponding physical spins must all point up.

This greatly simplifies the work we must do. Since we will perform a partial trace over all ancilla states, the reduced density matrix for the system will be

$$\rho_s = \sum_k^{2^N-1} \langle k| \Big(\sum_{i,j} c_i c_j^\dagger |\psi_s\rangle_i |\psi_a\rangle_i \langle\psi_a|_j \langle\psi_s|_j \Big) |k\rangle$$

Since $|\psi_a\rangle$ is a definite spin configuration for the ancilla (and therefore belongs to the Hilbert space for which we have represented the states in), the inner product $\langle\psi_{a_j}|k\rangle = \delta_{jk}$. Moreover, $\langle k|\psi_{a_i}\rangle = \delta_{ki}$ so that

$$\rho_s = \sum_k^{2^N-1} c_i c_j^\dagger |\psi_s\rangle_i \langle\psi_s|_j \delta_{jk}\delta_{ki} = \sum_k^{2^N-1} |c_k|^2 |\psi_s\rangle_k \langle\psi_s|_k$$

Let us take a step back and examine what we have found. For a system of spin-1/2's with L

sites, we entangle the middle spins with N ancilla by way of

$$|\psi\rangle = \cos(\alpha)|\uparrow\rangle_s|\downarrow\rangle_a - \sin(\alpha)|\downarrow\rangle_s|\uparrow\rangle_a$$

By finding the total state, $|\Psi\rangle$, as tensor product of the spin states at each site (for both the ancilla and physical spins), we realize that we may write $|\Psi\rangle$ as a sum of all possible ancilla spin configurations and their corresponding physical spin configurations. Upon computing the reduced density matrix for the system, we have found that it is diagonal in the representation of physical spin states.

To make this picture less abstract, consider a very simple example of 3 physical spins and a single ancilla entangled with the middle system spin. If we prepare the unentangled spins in an up position, and the entangled system/ancilla spin pair according to the above prescription, we would get an initial state:

$$|\Psi\rangle = |\uparrow_{s_0}\rangle \otimes \frac{1}{\sqrt{2}}\Big(\cos(\alpha)|\uparrow_{s_1}\rangle|\downarrow_a\rangle - \sin(\alpha)|\downarrow_{s_1}\rangle|\uparrow_a\rangle\Big) \otimes |\uparrow_{s_2}\rangle$$

Notice that we only have one spin-1/2 ancilla so that its Hilbert space is two states large (the spin can be up or down). We can then write our state in the following manner

$$|\Psi\rangle = \frac{1}{\sqrt{2}}\Big(\cos(\alpha)|\uparrow\uparrow\uparrow_s\rangle|\downarrow_a\rangle - \sin(\alpha)|\uparrow\downarrow\uparrow_s\rangle|\uparrow_a\rangle\Big)$$

which has a reduced system density matrix

$$\rho_s = \frac{1}{2}\Big(\cos^2(\alpha)|\uparrow\uparrow\uparrow_s\rangle\langle\uparrow\uparrow\uparrow_s| + \sin^2(\alpha)|\uparrow\downarrow\uparrow_s\rangle\langle\uparrow\downarrow\uparrow_s|\Big)$$

This holds generally for a larger number of ancilla. To find the initial state of our system, then, we are tasked with finding what the system spin configuration is for each ancilla spin configuration in the sum $|\psi\rangle = \sum_i c_i|\psi_s\rangle_i \otimes |\psi_a\rangle_i$ as well as the corresponding c_i. First, we construct the Hilbert space of ancilla spins in an identical manner to the physical spin case, and create a list of length $L - N$ to represent the unentangled up spins of our system. From the ancilla Hilbert space, determine the corresponding spin configuration in a binary representation. For each state, determine the physical spin configuration and its coefficient, $|c_k|^2$ as follows: Initialize $c_k = 1$. In the

ancilla configuration, i, if the spin at site j is down, multiply c_k by $\cos(\alpha)$. On the other hand, multiply c_k by $\sin(\alpha)$ if the spin is up. At the same time, create a list that will represent the entangled physical spin configuration for a particular ancilla configuration. For each site of the ancilla spins, if it is pointing down, append a 1 to the physical spin list (corresponding to a spin up), and append a 0 to the physical spin list if the ancilla spin is up. Finally, we can insert this new list of physical spins into the middle of our list of unentangled spins to generate a physical spin configuration. By doing this for all states in the ancilla Hilbert space, we will have all we need to construct $|\Psi\rangle$, and more importantly, ρ_s.

To create a matrix representation of ρ_s numerically, we need only loop through the physical states corresponding to the ancilla states that we found above. Since ρ_s acts on the system, it will be of size $2^L \times 2^L$. For each spin state in our generated subspace, determine its decimal representation, i, to find its place in the total physical Hilbert space. Then, the element $\rho_{s,(i,i)}$ will be equal to $|c_i|^2$ where c_i is the coefficient to the state calculated above. Note that not all of the diagonal components of ρ_s will be nonzero; some will be zero because the ancilla Hilbert space did not generate a physical spin configuration for all states in the physical space (it would be impossible to do this for $N < L$ since the Hilbert space dimensions do not match).

2.3.3 Time Evolution of Initial States

To ensure that there is nothing special about our initial state, we can rotate each spin about the x axis using the operator $R_z = e^{i\sum_j w_j S_j^x}$ where w_j are random angles taken from the uniform distribution $w_j \in [0, 2\pi]$. This can be done directly to the density matrix. Then, we would like to measure $\chi(t)$, where the reduced density matrix of the system, ρ_s evolves according to

$$\rho_s(t) = U_{edge} R_z \rho_s R_z^\dagger U_{edge}^\dagger$$

where $U_{edge} = \tau e^{-iH_{1d}t}$. Since we have constructed all of these quantities, we need only perform the matrix multiplication for each time step we wish to consider (though the spin rotation only needs to be performed once).

Note that the equation for χ in equation 2.2 depends on us knowing the reduced density matrices for the left side and right side of the system. All of our computations have been done in the

basis of physical spin configurations along z. Therefore, the system density matrix is

$$\rho_s = \sum_{i,j} \rho_{ij} |i\rangle\langle j|$$

even after the time evolution (the elements ρ_{ij} will be different from before). To compute the density matrix for the left side of the system, we start by numerically constructing the Hilbert space for the left and right side of the 1D system of size $2^{L/2}$ in the same fashion as we've already done (since our cut is in the middle of the system, these should be the same). Then, we can sum over all such states:

$$\rho_{s_L} = \sum_{k=0}^{2^{L/2}-1} \sum_{i,j}^{2^L-1} \rho_{ij} \langle k|i\rangle\langle j|k\rangle$$

For each element of the system density matrix, we loop over the right side Hilbert space states. Only one term in the sum over k will be nonzero for each element of ρ_s. If the left side spins (those from index 0 to $L/2-1$) of state $|i\rangle$ *and* state $|j\rangle$ match, then we add to ρ_{s_L} the term $\rho_{ij}|i_L\rangle\langle j_L|$ where $|i_L\rangle$ is the subsystem that is the left side spins of the full system spin state i. Numerically, the corresponding state vectors to use in finding ρ_{s_L} are found by matching the decimal representation of the binary spin states i_L and j_L to their position in the left system Hilbert space. This process can be carried out to find the left side density matrix, as well as the right side density matrix (with the simple change that we must instead sum over the left spins).

With these reduced density matrices at each time step, all that is left is to compute

$$\chi = S(s_L) - S(s_R) = \mathrm{tr}_{s_L}\left(\rho_{s_R} \log \rho_{s_R}\right) - \mathrm{tr}_{s_R}\left(\rho_{s_L} \log \rho_{s_L}\right).$$

The trace is basis independent, so we may either perform multiplications and sum the diagonal elements, or take a less computationally expensive approach and diagonalize the density matrices, giving

$$\chi = \sum_i \left(\lambda^i_{s_R} \log \lambda^i_{s_R} - \lambda^i_{s_L} \log \lambda^i_{s_L}\right) \tag{2.4}$$

for the eigenvalues, λ, of the matrices.

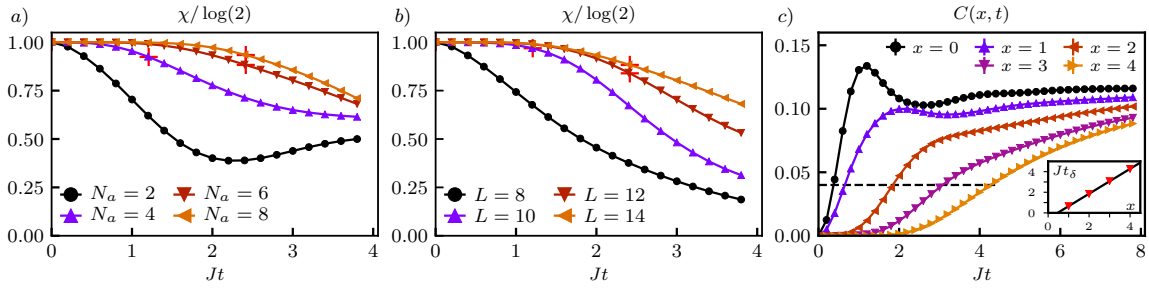

Figure 2.4.1: The above figure shows numerical results for a simulation of χ. In (a), the system size is fixed at $L = 14$ and the number of ancilla are varied between $N_a = 2$ and $N_a = 8$. In (b), the evolution is shown for fixed ancilla $N_a = 6$ and varying system size from $L = 8$ and $L = 14$. Both data sets show extended regions of quantization for larger ancilla/system size. In (c), the butterfly correlator is examined as a way to quantify the spread of entanglement in the chiral edge. Averaged over 100 disorder realizations, it tracks the influence of a spin at the beginning of the $1d$ chain on other spins. The inset shows the times, t_δ, at which each curve for a site x satisfies $C(x,t) = 0.04$. A linear fit allows for an approximation to the Lieb-Robinson velocity.

2.4 Numerical Simulations of Chiral Edges

The above numerical construction can be implemented to examine the dynamics of a purely $1d$ edge of a chiral Floquet phase. In particular, these results are shown in Fig. 2.4.1. Let us first consider the implications of Fig. 2.4.1a. The χMI, under the dynamics of $U = e^{-iHt_{1d}}\tau$ and H_{1d} given by Equation 2.3, is shown as a function of Floquet period, measured in units of Jt. Here the on-site potentials are drawn from a random uniform distribution, $h_i^{x/z} \in [-J, J]$.

The χMI is normalized by the ideal value of $\log 2$ and shown for a system size of $L = 14$. The total number of ancilla used to track the information transfer is varied between $N_a = 2$ and $N_a = 8$. Clearly, χ shows evidence of quantization to longer times with increasing ancilla number. That is, the more ancilla that are used to track the system states, the more persistent the quantization. This makes intuitive sense; the system spins that lie outside the ancilla covered region can spread entanglement past the cut, which would then be untracked information transfer. By using more ancilla, we increase the distance that untracked entanglement must spread.

Note, however, that the $N_a = 6$ and $N_a = 8$ curves show very similar quantization behavior. This is a byproduct of the periodic boundary conditions of our chain. The degradation of χ arises from the spread of untracked information over the entanglement cut, but the boundary conditions

produce a second cut that we haven't considered. Information wrapping around this direction can leak into the ancilla region and pull χ away from its ideal value.

We notice similar behavior in Fig. 2.4.1b, where we instead fix the ancilla number at $N_a = 6$ and vary the system size from $L = 8$ and $L = 14$. The argument used above to justify the similarity in curves for different ancilla numbers can be employed here for the similarities in the $L = 12$ and $L = 14$ curves. The shortest distance between an untracked system spin and an ancilla covered spin on the opposite side of our entanglement cut is the same for $N_a = 6$ and the two different system sizes. In the $L = 12$ case, the entanglement can spread to the right (in the sense of the top edge of Fig. 2.1.1), whereas it can spread to the left in the $L = 14$ case.

The result of this ancilla and system size dependence on the quantization of χ can be quantified. In particular, the optimal number of ancilla for a given system size, L, is set by the minimum distance between an untracked and tracked spin, ℓ_a. This quantity, given by

$$\ell_a = \min\left[\frac{N_a}{2} - 1, \frac{L - N_a}{2} - 1\right] \tag{2.5}$$

is the same of the two cases examined above. It can be used to understand the time at which we may expect a chiral edge (in the absence of bulk interactions) to exhibit persistent quantized information transfer. The finite speed of information propagation is captured by the Lieb-Robinson velocity, v_{LR}. It should therefore be expected that for times, t, satisfying $t \ll \ell_a / v_{LR}$, then χ will remain ideally quantized in finite size systems.

An approximation to the Lieb-Robinson velocity can also be extracted to examine the onset of deviations in χ. The butterfly correlator provides a means of doing this [35]. In particular, if we time evolve a Pauli operator, σ_i^z, at site i, then we want to know how much a spin state at site j as it was at time $t = 0$ has influenced the i spin. We can measure this with the butterfly correlator:

$$C(i, j; t) = -4\overline{\langle \left[e^{iHt} S_i^z e^{-iHt}, S_j^z(0)\right]^2 \rangle} \tag{2.6}$$

where the brackets indicate an average over states in the Hilbert space, and the bar indicates an average over disorder configurations. From the butterfly correlator, it's possible to estimate the Lieb-Robinson velocity of entanglement spreading [35]; by finding the time for which $C = \delta$, one may plot these times as a function of $|i - j|$, the inverse of the slope of which gives the butterfly

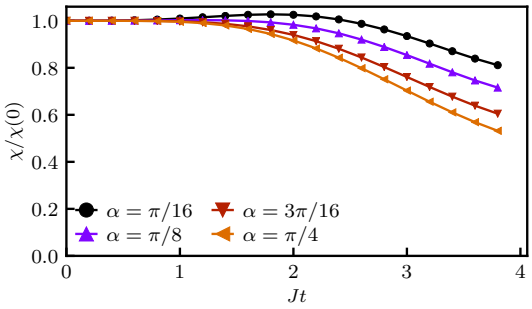

Figure 2.4.2: The above figure shows the effects of evolving χ for non-maximally entangled ancilla regions. With $L = 12$ spins and $N_a = 6$ ancilla, the results show that maximal entanglement may not be essential to the quantization of χ. The α parameters describe the precise entanglement between the ancilla and physical spins, which is taken to be uniform over the region.

velocity. This represents an appropriate estimate to the Lieb-Robinson velocity.

Figure 2.4.1c shows the correlator under the dynamics of equation 2.3, averaged over the entire Hilbert space and 100 disorder realizations. The dashed line represents a value $t^* = 0.04$. For sites $x = 1, 2, 3,$ and4, we can find the time t at which $t = t^*$ for that spin and plot as a function of spin site (note that $j = 0$ here). Fitting this to a line (shown in the Fig. 2.4.1c inset) allows us to estimate v_{LR}. Taking this quantity and plotting the times for which $v_{LR}t = \ell_a$ on Fig. 2.4.1a and Fig. 2.4.1b show quantitatively that the extended quantization and subsequent degradation of χ is brought on by the finite speed of entanglement propagation.

The above analysis was limited to an ancilla region that is maximally entangled with the system edge spins. At the present time, it is not clear whether or not maximal entanglement is an essential feature. Numerical results (see Fig. 2.4.2) suggest that so long as the entanglement is uniform over the ancilla region, the quantization of χ persists. Here we prepare each ancilla and corresponding system qubit in a state

$$|\psi\rangle = \cos(\alpha)|\uparrow_s\rangle|\downarrow_a\rangle - \sin(\alpha)|\downarrow_s\rangle|\uparrow_a\rangle$$

where α is an entanglement parameter. While the quantized value of χ changes due to a different amount of entanglement being transferred, this can be normalized to the ideal value. Figure 2.4.2

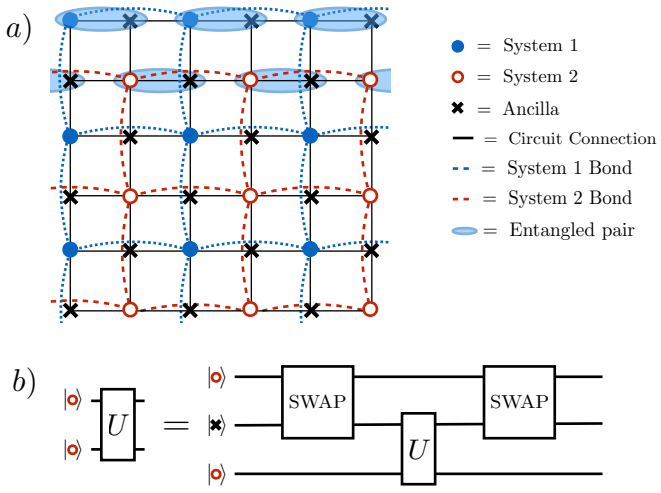

Figure 2.5.1: A proposed scheme for an experimental realization of the chiral mutual information is shown above. a) shows the physical qubit lattice, where four virtual layers of the system and ancilla have been compressed into the same plane. Note that the ancilla are nondynamical, and it is therefore unnecessary to distinguish between which systems they belong to. Initializing the entanglement as prescribed above is sufficient. To achieve a SWAP within a single system copy, for which two qubits are next-nearest neighbors on the physical lattice, the circuit in b) can be employed. Here the intervening ancilla is moved out of the way, and the system spins are allowed to evolve before replacing the position of the ancilla.

shows numerical simulations for a system of size $L = 12$ and $N_a = 6$ ancilla, with χ normalized to its initial (ideal) quantized value. For all entanglement parameters, there appears to be a clear region of quantization prior to degradation.

2.5 Experimental Realizations and Outlook

One of the primary motivations for introducing the chiral mutual information was to build a quantity that may be experimentally realizable. To this end, we note that the chiral mutual information can be formulated in terms of the nth order Renyi entropies instead of the von Neumann entropies. In this context, the above numerical and analytic results still hold. Let us refer to these new chiral

mutual information quantities as χ_n, corresponding to the nth order Renyi entropy:

$$S_n(A) = \frac{1}{1-n}\text{tr}\left(\log \rho_A^2\right)$$

In the case $n = 2$, previous works have established that these Renyi entropies can be measured experimentally [17, 18]. To do so, one requires two copies of the system with which the entropies are to be measured between [17, 18]. Given that one has this, an interference measurement can be made on the SWAP operator upon interchanging the copies of the system [17, 18].

For such an experimental realization to be made to measure χ_2, it would seem the most obvious choice of geometry is a four layer set up. This would give two copies of the system and two copies of the ancilla with which to perform interference measurements of the entropies. While this geometry may be plausible in trapped atoms, it still presents a technical challenge. Moreover, superconducting qubit arrays are of growing interest in quantum device physics, and these are restricted to two dimensional geometries.

An advantage to implementing a chiral Floquet phase on these arrays is that the qubits are coupled inductively with effective interactions governed by [36]

$$H = \frac{1}{2}\sum_{\langle i,j\rangle} J_{ij}(t)\left(S_i^+ S_j^- + S_i^+ S_j^-\right)$$

Such a Hamiltonian has the ability to realize chiral Floquet phases with a chiral unitary index of $\log 2$. We therefore would like to be able to implement the four layer geometry in these arrays of qubits.

To do this, we can utilize a planar geometry and use alternating qubits as the different system and ancilla copies. In particular, consider the implementation in Fig. 2.5.1a. The two copies of the system are arranged on alternating checkerboard latices, with the respective qubits being arranged in a '$+$' pattern, while the ancilla are arranged in a X pattern. Note that we have not distinguished between the different ancilla copies; such a distinction is not necessary since the ancilla are non-dynamical. However, they must be initially entangled with their system counterpart, and the appropriate interference measurements between ancilla must be made to appropriately measure χ.

To physically implement the CF model, consider the circuit in Fig. 2.5.1b. To interact two next neighboring qubits (neighbors in their respective system copy), we may perform a SWAP

between the intervening ancilla and one of the qubits, followed by the desired unitary; this can be an imperfect SWAP of the states, for example. Following the unitary evolution, the state of the ancilla can be put back in place with another SWAP. In these operations, it is important to consider the fidelity of the SWAP gate that is applied; we do not want additional entanglement dynamics to be generated between the system and ancilla.

These results are promising, and the possibility of an experimental realization is of great interest. Is a final point, we note a number of loose ends and present open questions that remain in this study. The analysis that we have presented has been restricted to the case of $\nu = \log 2$ for spin-1/2's. More generally, though, the analytic analysis did not appeal to this fact. The χMI works just as well for any ration chiral Floquet phase with $\nu = \log r$ for bosons.

However, it is presently unclear how or if this construction works for CF phases with topological order. It is well understood that the CF phase model can produce Abelian anyonic excitations [5, 7], and these models are characterized by unitary indices $\nu = \log \sqrt{r}$ for rational values of r. Because the bulk and edge dynamics do not actually decouple for these phases, the model we've used may not apply. It should be possible, in principle, to evolve such fractionalized phases over two periods, at which point the evolution will resemble the evolution of a bosonic model with twice as long of a drive period. The χMI may be interpreted for one period by dividing the measured chiral mutual information after $U(2T)$ by 2.

References

[1] C. Nayak, S. H. Simon, A. Stern, M. Freedman, and S. D. Sarma, Reviews of Modern Physics **80**, 1083 (2008).

[2] T. Kitagawa, E. Berg, M. Rudner, and E. Demler, Phys. Rev. B **82**, 235114 (2010).

[3] M. S. Rudner, N. H. Lindner, E. Berg, and M. Levin, Phys. Rev. X **3**, 031005 (2013).

[4] P. Titum, E. Berg, M. S. Rudner, G. Refael, and N. H. Lindner, Phys. Rev. X **6**, 021013 (2016).

[5] H. C. Po, L. Fidkowski, T. Morimoto, A. C. Potter, and A. Vishwanath, Phys. Rev. X **6**, 041070 (2016).

[6] F. Harper and R. Roy, Phys. Rev. Lett. **118**, 115301 (2017).

[7] H. C. Po, L. Fidkowski, A. Vishwanath, and A. C. Potter, Physical Review B **96**, 245116 (2017).

[8] L. Jiang, T. Kitagawa, J. Alicea, A. R. Akhmerov, D. Pekker, G. Refael, J. I. Cirac, E. Demler, M. D. Lukin, and P. Zoller, Phys. Rev. Lett. **106**, 220402 (2011).

[9] C. von Keyserlingk and S. Sondhi, Phys. Rev. B **93**, 245145 (2016).

[10] D. V. Else and C. Nayak, Phys. Rev. B **93**, 201103 (2016).

[11] A. C. Potter, T. Morimoto, and A. Vishwanath, Phys. Rev. X **6**, 041001 (2016).

[12] R. Roy and F. Harper, Phys. Rev. B **94**, 125105 (2016).

[13] R. Roy and F. Harper, Phys. Rev. B **96**, 155118 (2017).

[14] D. Gross, V. Nesme, H. Vogts, and R. Werner, Communications in Mathematical Physics **310**, 419 (2012).

[15] M. Burak Şahinoğlu, S. K. Shukla, F. Bi, and X. Chen, ArXiv e-prints (2017), arXiv:1704.01943 [quant-ph] .

[16] J. I. Cirac, D. Perez-Garcia, N. Schuch, and F. Verstraete, J. Stat. Mech. **2017**, 083105 (2017).

[17] P. Horodecki and A. Ekert, Phys. Rev. Lett. **89**, 127902 (2002).

[18] R. Islam, R. Ma, P. M. Preiss, M. Eric Tai, A. Lukin, M. Rispoli, and M. Greiner, Nature **528**, 77 (2015).

[19] R. Nandkishore and D. A. Huse, Annual Review of Condensed Matter Physics **6** (2015).

[20] D. M. Basko, I. L. Aleiner, and B. L. Altshuler, Annals of Physics **321** (2006).

[21] B. Bauer and C. Nayak, Journal of Statistical Mechanics: Theory and Experiment **2013**, P09005 (2013).

[22] A. Pal and D. A. Huse, Phys. Rev. B **82**, 174411 (2010).

[23] V. Oganesyan and D. A. Huse, Phys. Rev. B. **75** (2007).

[24] M. Serbyn, Z. Papić, and D. A. Abanin, Phys. Rev. Lett. **111**, 127201 (2013).

[25] D. A. Huse, R. Nandkishore, and V. Oganesyan, Phys. Rev. B. **90** (2014).

[26] B. R. Duschatko, P. T. Dumitrescu, and A. C. Potter, ArXiv e-prints (2018), arXiv:1804.02004 [cond-mat.str-el] .

[27] D. A. H. V. Oganesyan, Phys. Rev. B. **90** (2013).

[28] Phys. Rev. Lett. **114** (2015).

[29] R. Nandkishore and D. A. Huse, Ann. Rev. Cond. Matt. Phys. **6**, 15 (2015).

[30] E. Altman and R. Vosk, Annu. Rev. Condens. Matter Phys. **6**, 383 (2015).

[31] A. Lazarides, A. Das, and R. Moessner, Physical review letters **115**, 030402 (2015).

[32] P. Ponte, Z. Papić, F. Huveneers, and D. A. Abanin, Physical review letters **114**, 140401 (2015).

[33] E. H. Lieb and D. W. Robinson, Communications in Mathematical Physics **28** (1972).

[34] A. W. Sandvik, "Exact diagonalization studies," (2009).

[35] S. H. Shenker and D. Stanford, Journal of High Energy Physics **2014**, 67 (2014).

[36] P. Roushan, C. Neill, J. Tangpanitanon, V. M. Bastidas, A. Megrant, R. Barends, Y. Chen, Z. Chen, B. Chiaro, A. Dunsworth, A. Fowler, B. Foxen, M. Giustina, E. Jeffrey, J. Kelly, E. Lucero, J. Mutus, M. Neeley, C. Quintana, D. Sank, A. Vainsencher, J. Wenner, T. White, H. Neven, D. G. Angelakis, and J. Martinis, Science **358**, 1175 (2017).